Application of Vertical Nesting within ARW-WRF V3.2 to a Study of Highway Noise Pollution in Phoenix Arizona

S. R. Shaffer[1], M. Moustaoui[1], and A. Mahalov[1]

[1]Center for Environmental Fluid Dynamics, Department of Mechanical Engineering, Arizona State University, Tempe, AZ 85287-9809

Abstract

We apply the new option of vertical nesting implemented in ARW-WRF V3.2 within the finest nest for a numerical experiment studying highway noise pollution in the Phoenix metropolitan area. Vertical profiles are extracted having near-ground resolution finer than 20 m for input into a sound propagation model to produce forecasts of noise pollution from a highway line segment noise source. We demonstrate that vertical nesting improves the resolution of finer structures in the temperature and velocity profiles such as morning temperature inversions and low level jet-like features. A previous study by Ovenden, Shaffer and Fernando (2009) demonstrated the sensitivity of the resultant sound field within 600 m of the source to input effective sound speed vertical profiles, $C_{eff}(z)$, in the lowest 300 m of the planetary boundary layer. Hence, resolution of such features is important when forecasting $C_{eff}(z)$ for use in the highway noise propagation model. We use the field experiment case from OSF09 of 7 November 2006 during 7:40 to 8:00 a.m. in Phoenix as a reference for comparison.

1 Introduction

The latest version of the Advanced Research Weather Research and Forecasting model [10] released on 2 April 2010 ARW-WRF v3.2 has the capability of refining the vertical grid resolution within a child domain, making possible the study of detailed phenomenon and enabling further application of the model output data in a limited area, without the computational expense of running all nests at the higher resolution [2].

Highway noise pollution has been associated with many adverse affects ranging from human health [4, 7] and housing prices [5] in populated urban and sub-urban settings to wildlife [8, 1] in more remote areas. The predictability of such environmental factors in an urban setting is of interest given the rate of urban growth both in terms of population and land use type as the current world population is rapidly moving away from rural lifestyles [3]. It is of interest to city planners to account for noise, deemed as undesired sound, when designing transportation systems and to consider mitigation for improving areas already receiving complaints of traffic noise, or for being in violation of the Federal Highway Noise Abatement Criterion when exceeding 67 dBA, where A-weighting is used to represent human sensitivity to hearing by applying a band-pass-filter.

A previous study by the author showed that knowledge of the near-ground profiles of temperature and wind speed in the direction of sound propagation, taken transverse to the roadway, are crucial for predicting sound propagation from a highway (OSF09 [6]). It is desirable to forecast these profiles for both future studies, and for back-casting to perform re-analysis of previous studies which may have not accounted for the full meteorological profile. We demonstrate the degree of representativeness that can be attained from utilizing vertical nesting to 81 levels from 27, at 1 km horizontal resolution, in comparison with results of case B from OSF09.

The organization of this paper is as follows. The sound model numerical experiment is presented in §2 with the WRF configuration in §2.1, a description of the sound model in §2.2, the selection process for WRF profiles in §2.3 with the profiles given in §2.4 and results of the sound model in §2.5, followed by discussion and conclusions in §3 and future work in §4.

Figure 1: WRF Model Domain as generated using WRF Domain Wizard using 4 nests centered on Phoenix, Arizona with horizontal resolutions of 27, 9, 3 and 1 km.

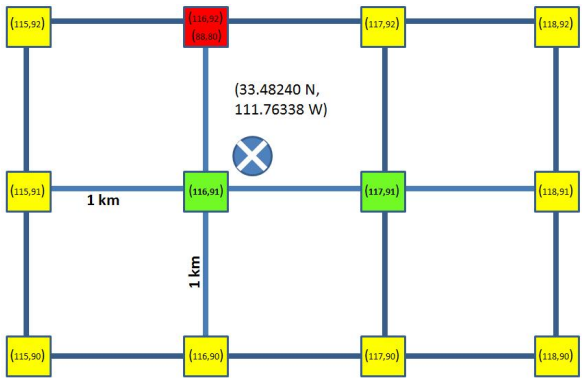

(a) Schematic

(b) Google Earth background

Figure 2: WRF computational domain for Arkawa-C staggered grid cell center locations in the neighborhood of the site location (blue - coordinates given in degrees Latitude and Longitude) as a schematic diagram (a) and Google map (b). Squares show model grid coordinates of neighboring WRF grid points for the 1km grid (yellow), closest on 1km grid (green) and closest on 3km grid (red-coincident with a yellow). North is up for both figures.

2 Sound Model Numerical Experiment

2.1 WRF Model Domain

The domain used for both studies consists of four nests shown in Figure 1, all centered on Phoenix Arizona, with horizontal resolutions of 27, 9, 3 and 1 km. There were 27 vertical levels used for all nests except the fourth, which used 81 vertical levels. For both studies, the physics and dynamics options were set to the values given in the Appendix 2.

2.2 PE Sound Model

We use the same model as presented in OSF09, a summary of which is provided here. The highway is treated as a series of mono-frequency coherent effective line-sources above a fixed lane, a reasonable approximation when considering 20 minute time-averaged sound levels, and the ground is treated as an impedance plane. A spectral model called the wide-angle Parabolic Equation (PE) approximation [9] is used to model one-way sound propagation from a profile of complex pressure. The PE model is derived by splitting the 2-D Cartesian Helmholtz wave equation into two one-way propagation operators and considering only waves moving in one direction within a 2-D plane transverse to a line source. An absorbing layer at the model top boundary prevents artificial numerically reflected waves.

Stability of the PE model requires 10 points per wavelength, so high frequencies become costly to compute. Restricting the acoustic spectrum to 17 standard third-octave frequency bands incurs less than 1% error due to A-weighting when compared to the sum over any larger bandwidth and speeds computation time by eliminating higher frequencies. Each third-octave band's central frequency is assumed to represent the entire band, so the logarithmic-sum of the PE calculations for each band gives the resultant total field.

The model input is the starting pressure field and the effective-sound-speed profile up to 300 m above ground level (AGL), defined as,

$$C_{eff}(z) = \sqrt{\gamma RT(z)} + U_{\|}, \qquad (1)$$

where γ is the ratio of specific heats, R is the gas constant, $T(z)$ is the temperature profile and $U_{\|}(z)$ is

the profile of fluid flow speed parallel to the direction of propagation. The first term is commonly referred to as the adiabatic sound speed, C_{ad} (also given by $C_{ad}(z) = 331.3\sqrt{T(z)/273.15}$ m s^{-1} for temperature T in Kelvin) and the second term accounts for advection. The source heights and strengths were kept the same as for Case B in OSF09. A Green's function solution for an infinite line above an impedance plane is used to obtain the starting pressure field for the PE model at the edge of the roadway, where the ground impedance value changes from one representative of asphalt, to that of hard sandy soil typical for the site location. Atmospheric absorption is applied to each frequency band after the PE model gives output.

2.3 Site Location and profile selection

The site adjacent to highway Loop 202 in the East Phoenix Metropolitan area used for previous studies in OSF09 is located at approximately 33.48240 N latitude and 111.76338 W longitude, as denoted in Figure 2 by a blue marker. The schematic in Figure 2a for the 1 km resolution WRF grid center locations show the two closest points in green and the 10 nearest neighbors in yellow, except for the one red point being the nearest grid location for the 3 km nest. These are overlaid on a Google Earth image in Figure 2b giving an indication of the land use for this area. Based upon these grid locations and with the highway running primarily East-West, profiles of potential temperature and V velocity are extracted to generate the input $C_{eff}(z)$ profiles used in the PE model. We denote by C^{-}_{eff} when looking against the V component (e.g. $C^{\pm}_{eff} = C_{ad} \pm V$).

2.4 Input Meteorological Profiles derived from WRF

Case B in OSF09 is between 0740 and 0800 local time on 7 November 2006. The WRF run was begun at UTC 0500 on 5 November 2006 to allow sufficient spin-up time. Profiles were then extracted at 1200 UTC on 7 November 2006 as representative of the morning inversion, and used to derive C_{eff}. The temperature was obtained by,

$$T = (\theta' + \theta) \cdot ((P' + \bar{P})/P_0)^{R/c_p}, \qquad (2)$$

where $\theta = 300$ K the base potential temperature, θ' is the perturbation potential temperature,

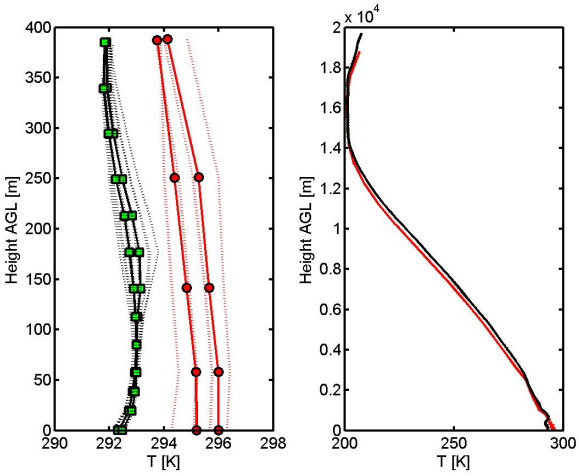

Figure 3: Temperature profile derived from potential temperature for the 27 vertical level 3x3 km grid (red) and the 81 vertical level 1x1 km grid (black) for closest grid points (green) and nearest neighbors (dashed) for the lowest 400 meters (left) and the full vertical extent of ≈20km (right). Vertical levels are indicated by green squares (lowest 13 of 81) and red circles (lowest 5 of 27) in the left panel for the two profiles closest to the site.

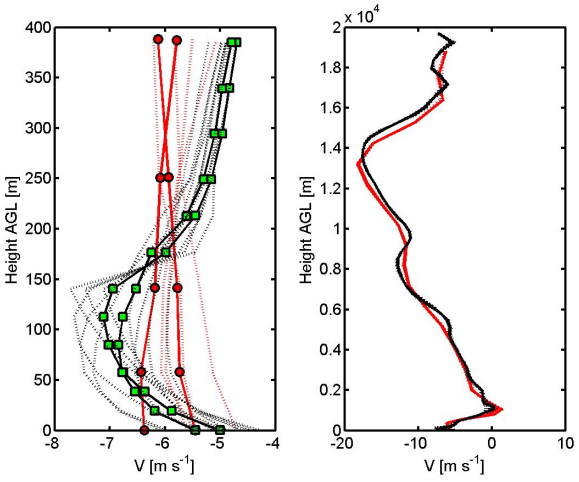

Figure 4: Same as Figure 3 but for V component of horizontal velocity. Note that negative values are towards the South.

$P_0 = 10000$ Pa is the reference pressure, $P' + \bar{P}$ the perturbation plus base pressure and $R/c_p = 8.314472/29.07$ is the ratio of gas constant to specific heat at constant pressure. Profiles of derived temperature and V velocity are shown in Figures 3

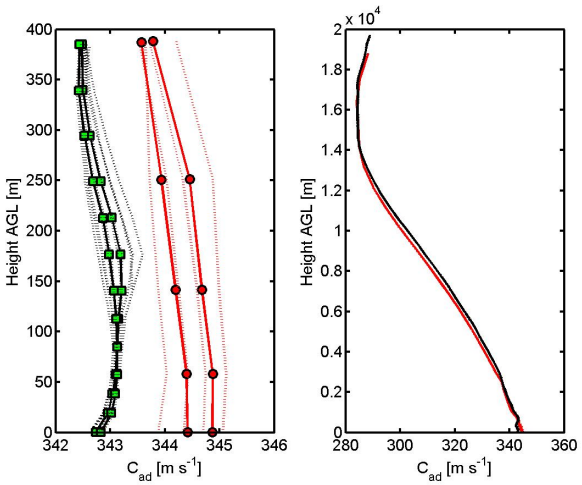

Figure 5: Same as Figure 3 but for adiabatic sound speed derived from potential temperature by equation 2.

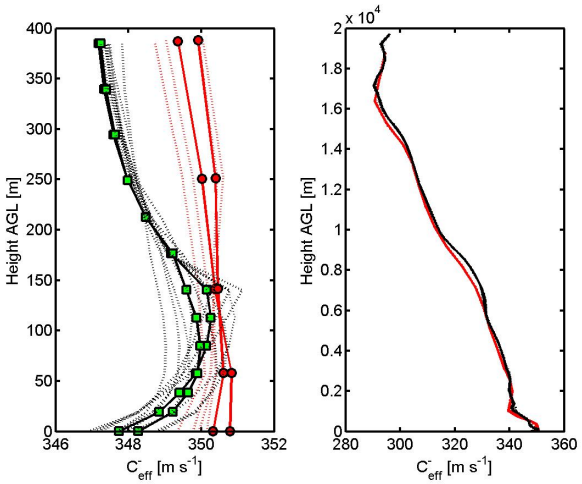

Figure 6: Same as Figure 3 but for effective sound speed C_{eff}^{-} on looking down-wind towards the South side of the highway.

and 4 respectively. In each of the profile plots, the full 20 km vertical extent is shown in the right panel with only the 400 m nearest the ground in the left panel. The red line corresponds to the 27 vertical level profile on the 3 x 3 km grid (red point in Figure 2). Likewise, the green points mark the closest points on the 81 vertical level 1 x 1 km grid. All the black dashed curves are the nearest neighbors in the 81 vertical level resolution and red dashed are for the 27 vertical level. The adiabatic and effective sound speeds shown respectively in Figures 5 and 6 are computed using equations 1 and 2 which are then interpolated with cubic splines to the resolution needed for the sound model for each frequency.

2.5 PE Model Results

The PE model was used to calculate the total sound field based upon the C_{eff} profiles extracted. A spectrum versus range at 1 m AGL is then obtained. Shown in Figure 7 is the neutral case, a control where the velocity is set to zero and the temperature profile is held fixed at the ground value. Contrast this with Figures 8 and 9, the spectral-range plots for the 27 and 81 vertical level profiles of C_{eff}^{-}, respectively, closest to the site location.

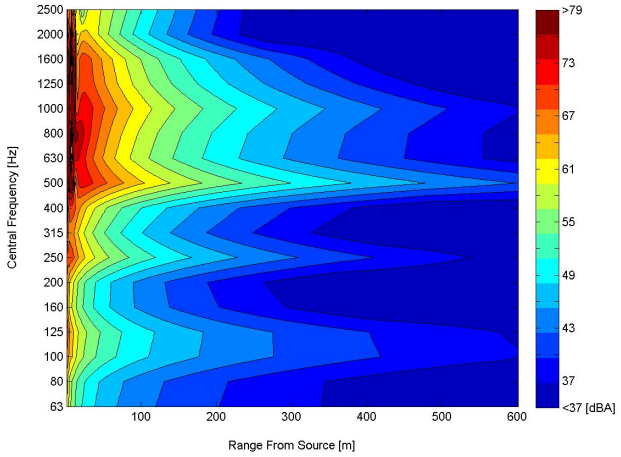

Figure 7: A-weighted spectrum [dBA] versus range at 1 meter AGL. Here for the neutral case using the ground level temperature from the 27 vertical level experiment on the 3km horizontal grid. The 81 vertical level neutral case (not shown) is similar (because the vertical gradient is also zero) but shifted due to a different temperature giving a different uniform adiabatic sound speed. Contours are in intervals of 3 dBA, consistent with a doubling of distance from a line source yielding half of the sound pressure level.

Finally, to comparatively display the degree of representativeness between the C_{eff}^{-} profiles used, we show an attenuation versus range plot at 1 m AGL. Although identical in each case, the source strength is effectively removed by computing the sound pressure level summed over all 17 third-octave bands, with respect to the value at 50 m range. The offset between the neutral attenuation curve for each case and that from Case B of OSF09 is used to shift the

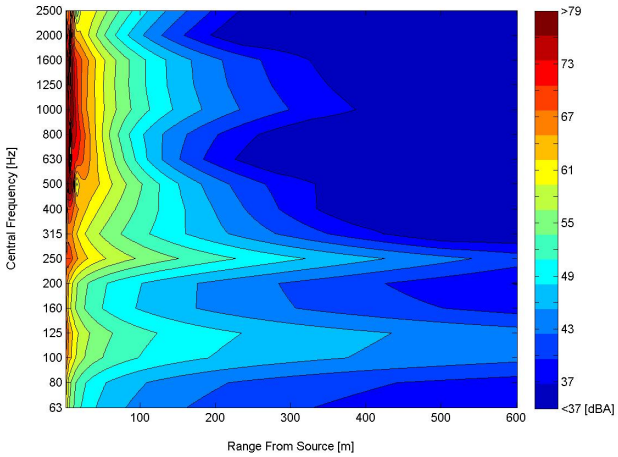

Figure 8: Same as Figure 7 but here for the 27 vertical level with 3km horizontal simulation using C_{eff}^{-}.

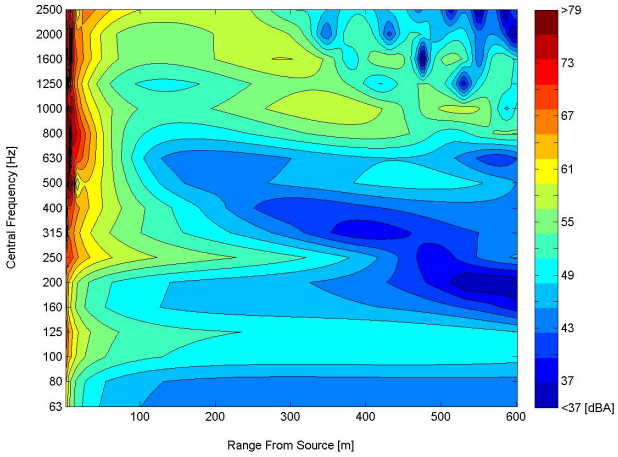

Figure 9: Same as Figure 8 but here for the 81 vertical level with 1km horizontal simulation using C_{eff}^{-}.

respective attenuation curve which uses C_{eff}^{-}. This offset subtraction ensures that all attenuation versus range plots have the same zero point, so direct comparisons of the results shown in Figure 10 can be made.

3 Discussion and Conclusions

Reproduced in Appendix 1 are Figures A.1, A.2 and A.3 showing profiles of T, -V and Ceff along with the third-octave spectrum versus range at 1 m AGL plots from Case B of OSF09 for ease of comparison. Examining Figure 10, the approximately 10

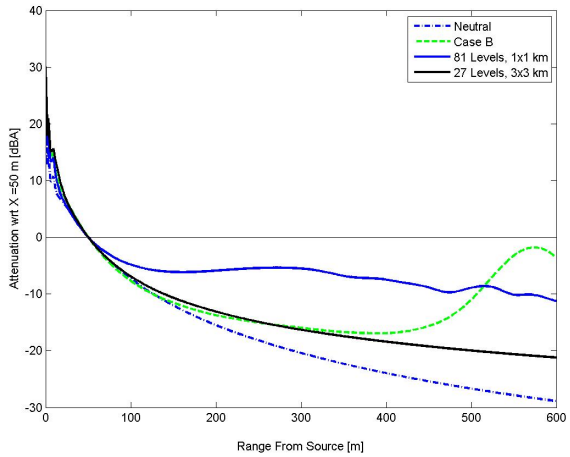

Figure 10: Attenuation of total A-weighted sound field relative to 50m in range versus range from source, at 1m AGL. The dashed blue curve is for the neutral Case B with constant temperature and zero winds, the black curve is for 27 vertical levels on the 3x3 km horizontal grid using C_{eff}^{-}, the solid blue curve is for 81 vertical levels on the 1x1 km horizontal grid, also with C_{eff}^{-} and the dashed green curve is from Case B of [6], again with C_{eff}^{-} for that case being used.

dBA difference in attenuation of the total sound field is quite apparent beginning around 100 m in range between the higher resolution WRF simulation and other cases. The input profile from the 27 vertical level WRF simulation, though different from the neutral case indicating some refractive effects, is still not as significant as for the 81 vertical levels. Though neither has the same form as case B, where near-ground upward refraction was overcome downrange due to stronger elevated downward refracting conditions. Though some of these effects measured in the field could be due to bottom boundary conditions not realized in the 1 km x 1 km grid used in the WRF model. For instance, details of the flow due to terrain and land-use classification may not be present, which if accounted for could lead to a closer representation of the actual measured profile. Without higher resolution surface boundary data, it is not reasonable to increase the resolution of the WRF domain, and so parameterizations need to be explored.

Examining Figures 7 and 8, the 27 vertical layer is not too unlike a neutral or limited refracting

atmosphere, as expected from the nearly zero to slightly negative vertical gradient of the effective sound speed in Figure 6. The frequencies around 400 to 1000 Hz are suppressed near the ground, indicating slight upward refraction combined with the response curve of atmospheric absorption, they would be highly attenuated. Meanwhile the lower frequencies around 100 Hz are enhanced, so lower absorption combining with some refraction leads to the enhanced sound levels at these lower frequencies. However, when examining the 81 vertical level case in Figure 9, it seems apparent that downward refraction is taking place, increasing the levels of the 800 and 1000 Hz bands significantly out to 600 m range. Similar phenomenon is seen, though significantly stronger in both Case A (not reproduced) and B of OSF09 when the vertical gradient of Ceff is positive. The additional features in the observational profile near the ground, as explained in OSF09, cause upward refraction, which explains the quiet zone around 300 m range in Figure A.3. These details in the profiles are likely due to local terrain features not represented in the 1km WRF grid. So although profiles representative of inversions and jet-like features are present, and do produce significant differences between the 81 vertical level nest compared to 27 levels, yet more realistic profiles are still needed to reproduce the sound field generated by the observed profiles at mid-range. However, the increased sound levels near 600 m range for bands near 1000 Hz are present, though not as enhanced.

In summary, we have shown that conditions of morning temperature inversion and low-level jet or wind shear can be reasonably reproduced using WRF with increased vertical levels – and more efficiently with the use of vertical nesting, compared to using fewer vertical levels in the model. Further, that these profiles can be used to generate sound fields representative of expectations from observation. However, more detailed structures of the profiles are still needed, which would require higher resolution information about the terrain or some form of sub-grid parametrization scheme.

4 Future Work

Shown here are only the results from the closest profile. The attenuation versus range plot for each neighboring profile will be computed to generate an ensemble of profiles representative of the site location and to generate statistics for the data shown in Figure 10 and for 27 levels on the 1 km grid. Implementation of various PBL schemes will be explored to see if more realistic flow details can be observed.

Acknowledgments

This work was supported by NSF CMG grant ATM-0934592 and by the Arizona Department of Transportation. The author would also like to thank Christ Dimitroplos and H.J.S. Fernando for their support of this work. The data for this study are from the Research Data Archive (RDA) which is maintained by the Computational and Information Systems Laboratory (CISL) at the National Center for Atmospheric Research (NCAR). NCAR is sponsored by the National Science Foundation (NSF). The original data are available from the RDA (`http://dss.ucar.edu`) in dataset number ds083.2.

References

[1] Richard T. T. Forman and Robert D. Deblinger. The ecological road-effect zone of a massachusetts (u.s.a.) suburban highway. *Conservation Biology*, 14(1):36–46, 2000.

[2] Alex Mahalov and Mohamed Moustaoui. Vertically nested nonhydrostatic model for multiscale resolution of flows in the upper troposphere and lower stratosphere. *Journal of Computational Physics*, 228(4):1294 – 1311, 2009.

[3] E. L. Moreno, N. Bazoglu, G. Mboup, and R. Warah. *State of the World's Cities 2008/2009: Harmonious Cities*. UN-HABITAT, 2008.

[4] Anne Vernez Moudon. Real noise from the urban environment: How ambient community noise affects health and what can be done about it. *American Journal of Preventive Medicine*, 37(2):167 – 171, 2009.

[5] Jon P. Nelson. Highway noise and property values: A survey of recent evidence. *Journal of Transport Economics and Policy*, 16(2):117–138, 1982.

[6] N.C. Ovenden, S.R. Shaffer, and H.J.S. Fernando. Impact of meteorological conditions

on noise propagation from freeway corridors. *Journal of the Acoustical Society of America*, 126:25–35, July 2009.

[7] W. Passchier-Vermeer and W. F. Passchier. Noise exposure and public health. *Environmental Health Perspectives*, 108:123–131, 2000.

[8] F. E. Rheindt. The impact of roads on birds: Does song frequency play a role in determining susceptibility to noise pollution? *Journal of Ornithology*, 144:295–306, 2003.

[9] E.M. Salomons. *Computational Atmospheric Acoustics*. Kluwer Academic Publishers, 2001.

[10] W. C. Skamarock and J. B. Klemp. A time-split nonhydrostatic atmospheric model for weather research and forecasting applications. *Journal of Computational Physics*, 227:3465–3485, 2008.

Appendix 1: OSF09 Comparison Data

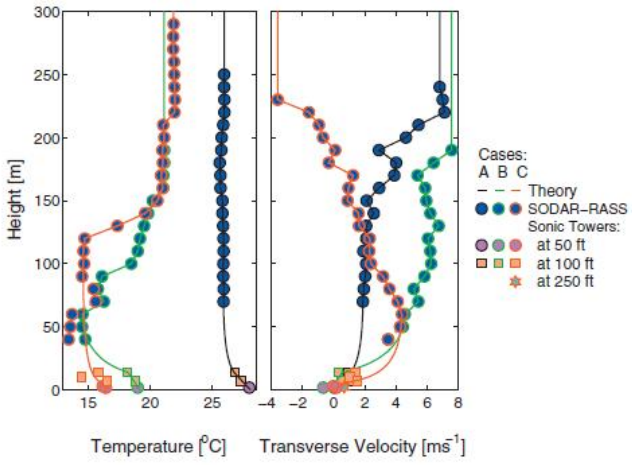

Figure A.1: Profiles of T and -V from OSF09. Case B is in green.

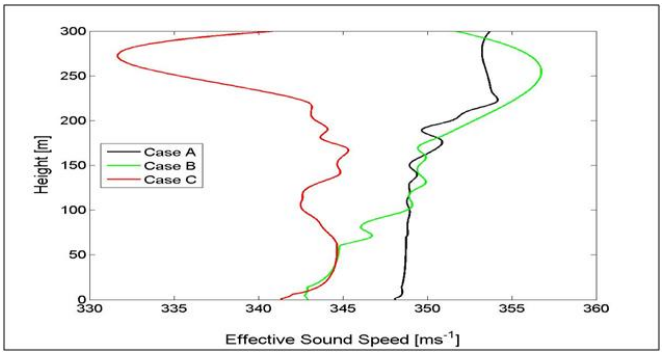

Figure A.2: Profiles of Ceff derived from OSF09 data. Case B is in green.

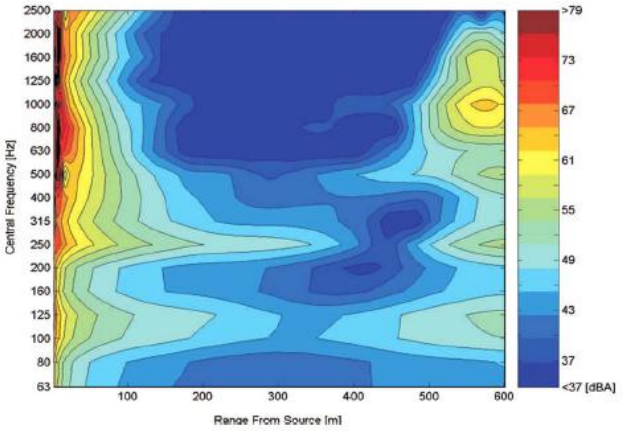

Figure A.3: Case B spectral sound level versus range at 1 m AGL from OSF09.

Appendix 2: namelist.input physics and dynamics sections

```
&physics                          &dynamics
mp_physics                = 3,    w_damping               = 0,
ra_lw_physics             = 1,    diff_opt                = 1,
ra_sw_physics             = 1,    km_opt                  = 4,
radt                      = 30,   diff_6th_opt            = 0,
sf_sfclay_physics         = 1,    diff_6th_factor         = 0.12,
sf_surface_physics        = 1,    base_temp               = 290.,
bl_pbl_physics            = 1,    damp_opt                = 0,
bldt                      = 0,    zdamp                   = 5000.,
cu_physics                = 1,    dampcoef                = 0.01,
cudt                      = 5,    khdif                   = 0,
isfflx                    = 1,    kvdif                   = 0,
ifsnow                    = 0,    smdiv                   = 0.1,
icloud                    = 1,    emdiv                   = 0.01,
surface_input_source      = 1,    epssm                   = 0.1,
num_soil_layers           = 5,    time_step_sound         = 4,
sf_urban_physics          = 0,    h_mom_adv_order         = 5,
mp_zero_out               = 0,    v_mom_adv_order         = 3,
maxiens                   = 1,    h_sca_adv_order         = 5,
maxens                    = 3,    v_sca_adv_order         = 3,
maxens2                   = 3,    non_hydrostatic         = .true.,
maxens3                   = 16,   moist_adv_opt           = 1,
ensdim                    = 144,  scalar_adv_opt          = 1,
                                  chem_adv_opt            = 1,
                                  tke_adv_opt             = 1,
```